Macedonian Journal of Chemistry and Chemical Engineering, Vol. **43**, No. 1, pp. 137–148 (2024)

MJCCA9 – 901

ISSN 1857-5552
e-ISSN 1857-5625

Received: April 4, 2024
Accepted: April 26, 2024

DOI: 10.20450/mjcce.2024.2861
Original scientific paper

SYNTHESIS, CHARACTERIZATION, AND VOLTAMMETRIC STUDY OF DIMETHYLAMMONIUM LEAD IODIDE PEROVSKITE[1]

Jeta Sela[1], Leon Stojanov[2], Besarta Cheliku Ramadani[1], Miha Bukleski[2], Arianit A. Reka[1], Sandra Dimitrovska-Lazova[2], Valentin Mirčeski[2, 3], Slobotka Aleksovska[2*]

[1]*Department of Chemistry, Faculty of Natural Sciences and Mathematics, University of Tetovo, Tetovo, Republic of N. Macedonia*
[2]*Institute of Chemistry, Faculty of Natural Sciences and Mathematics, Ss. Cyril and Methodius University in Skopje, Skopje, Republic of N. Macedonia*
[3]*Research Center for Environment and Materials, Macedonian Academy of Sciences and Arts, Skopje, Republic of N. Macedonia*

bote@pmf.ukim.mk

In the last decade, the most investigated perovskite materials are the hybrid organic-inorganic perovskites (HOIPs) due to their optoelectronic properties and possible application in the production of photovoltaics. This interest has led to an ongoing search for new HOIP variants, alongside thorough investigations of the properties of existing HOIPs. That is why our research in the field of organic-inorganic perovskites is aimed at the synthesis, characterization, and investigation of the electrochemical properties of dimethylammonium lead iodide ($DMAPbI_3$) using voltammetric studies. A modified synthesis of $DMAPbI_3$, differing slightly from the one described in the literature, was performed by combining stoichiometric amounts of lead iodide (PbI_2) and dimethylammonium iodide (DMAI) dissolved in acetonitrile. After conducting controlled evaporation, a yellow crystalline powder of $DMAPbI_3$ was obtained. The identity and purity of the obtained compound were confirmed by powder X-ray diffraction (PXRD), infrared (IR) and Raman spectroscopy, and scanning electron microscopy (SEM) with energy dispersive X-ray spectroscopy (EDX). Investigations on the electrochemical properties of $DMAPbI_3$ by cyclic voltammetry were performed with dichloromethane (DCM) and tetrabutylammonium chloride (TBAC) as the electrolyte. A paraffin-impregnated graphite electrode (PIGE) was used as a working electrode, on which the perovskite microparticles were immobilized. The electrochemical activity of $DMAPbI_3$ is recognized through an intense, broad, and irreversible anodic peak attributed to the oxidation of the constituents to different possible products and the decomposition of the perovskite structure.

Keywords: dimethylammonium lead iodide; cyclic voltammetry; PXRD; vibrational spectroscopy; SEM-EDX

СИНТЕЗА, КАРАКТЕРИЗАЦИЈА И ВОЛТАМЕТРИСКО ИСТРАЖУВАЊЕ НА ПЕРОВСКИТ НА ДИМЕТИЛАМОНИУМ ОЛОВО ЈОДИД

Во последнава деценија најистражуваните перовскитни материјали се хибридните органско-неоргански перовскити (HOIPs) поради нивните оптоелектрични својства и можната примена во производството на фотоволтаици. Интересот за нив доведе до постојано барање нови варијанти на HOIPs, истовремено со детални истражувања на својствата на веќе постојните. Затоа нашето истражување во областа на органско-неорганските перовскити е насочено кон синтеза, карактеризација и истражување на електрохемиските својства на диметиламониум олово јодид ($DMAPbI_3$) со примена на волтаметриско проучување. За таа цел беше изведена модифицирана синтеза на $DMAPbI_3$, малку различна од таа опишана во литературата, тргнувајќи од стехиометриски количества на оловојодид (PbI_2) и диметиламониумов јодид (DMAI) растворени во ацетонитрил. Со контролирано испарување беше добиен жолт кристален прашок од $DMAPbI_3$.

[1] Dedicated on the occasion of the Golden Jubilee of the *Macedonian Journal of Chemistry and Chemical Engineering*

Идентитетот и чистотата на добиеното соединение беа потврдени со прашковна рендгенска дифракција (PXRD), инфрацрвена (IR) и раманска спектроскопија и скенирачка електронска микроскопија (SEM) со енергетско-дисперзиона рендгенска спектроскопија (EDX). Истражувања на електрохемиските својства на $DMAPbI_3$ со циклична волтаметрија беа изведени во дихлорометан (DCM) и тетрабутиламониум хлорид (TBAC) како електролит. Како работна електрода беше користена графитна електрода импрегнирана со парафин (PIGE), на која беа имобилизирани микрочестички од перовскитот. Електрохемиската активност на $DMAPbI_3$ беше забележана преку еден интензивен, широк и иреверзибилен аноден пик, кој ѝ се припишува на оксидацијата на конституентите до различни можни продукти следена со разложување на перовскитната структура.

Клучни зборови: диметиламониум олово јодид; циклична волтаметрија; PXRD; вибрациона спектроскопија; SEM-EDX

1. INTRODUCTION

Over the past few decades, perovskite-type compounds (ABX_3) have become the focus of extensive research. The significant scientific attention directed towards these compounds arises from their adaptability, specifically in terms of composition and structure, giving rise to a multitude of valuable and distinctive characteristics that have diverse applications across various technical domains.[1–3] Perovskites have found applications in various fields, with their most notable breakthroughs occurring in the field of photovoltaics. Beyond photovoltaics, perovskites also exhibit many interesting properties, facilitating their use in other areas such as light-emitting diodes (LEDs), sensors, catalysts, and superconductors.[4]

As mentioned, the key feature of perovskites is their remarkable structural flexibility, which allows for the incorporation of a wide range of elements into the perovskite structure, resulting in a diverse family of materials.[5] Traditionally, the field of materials chemistry has been divided into organic and inorganic systems. However, in the last few decades, a new class of materials, often referred to as hybrid organic-inorganic frameworks, has attracted considerable attention as their vast structural and chemical diversity leads to potential technological applications beyond either purely organic or inorganic systems.[6,7] Hybrid organic-inorganic perovskites (HOIPs) are a subclass of the perovskite family, in which the A-site is occupied by an organic cation, the B-site contains a divalent metal cation, and in most cases, the X-site contains a halogen anion. Research into HOIPs has attracted a lot of attention recently in both the materials science and renewable energy communities, a consequence of their intriguing properties, which leads to applications in solar cell construction. In this respect, the most investigated HOIP is methylammonium lead iodide ($MAPbI_3$).[8] The cubic perovskite structure of $MAPbX_3$ (X = I, Br, and Cl) was first reported by Weber in 1978.[9] However, studies of these materials for optoelectronic devices did not start until the 1990s. Developed by Mitzi *et al*. at IBM,[10,11] a range of semiconducting perovskite-like materials with remarkable structural versatility have been innovated for applications in optoelectronics, including light-emitting diodes (LEDs) and transistors.[12,13] On the other hand, the exceptional utility of hybrid halide perovskites for photovoltaic applications started in 2009, when a photoelectrochemical cell incorporating a layer of $MAPbI_3$ as a visible light sensitizer was reported by Kojima *et al*. The initial power conversion efficiencies (PCEs) were 3.1 % and 3.8 % for $MAPbBr_3$ and $MAPbI_3$, respectively.[14] The intensive work in this field has led to a significant increase in PCE, reaching up to 30 % in just a few years.[4]

A recent investigation on organic-inorganic perovskites has shown that the organic cation in the structure has a great influence on both stability and performance.[15] Therefore, several attempts were made to exchange and modify the monovalent organic cation. The most investigated organic cation for the substitution of the methylammonium (MA) ion has been the formamidinium (FA) ion, *i.e.*, $CH(NH_2)_2^+$. $FAPbI_3$ is more thermally stable than both $MAPbI_3$ and $MAPbBr_3$, strongly supporting the findings that a larger cation at the A-site in the ABX_3 structure could further stabilize the perovskite structure.[16] Also, a number of HOIPs with mixed A-site cations in different molar ratios were synthesized and investigated.[17] In addition to A-site doping, B-site doping has also shown positive effects on both the performance and stability of perovskite-based optoelectronic devices.[17] Mixed $MAPb_{1-x}Mn_xI_3$ perovskites have suitable bandgaps and promising absorption coefficients, indicating promising potential for application in perovskite solar cells.[18] Lui *et al*.[19] investigated the role of the anion on the stability of the perovskite and the effi-

ciency of the solar cells. With an increase in the ionic size of the halide, the band gap energy is decreased, but the stability of the perovskite is increased with decreasing of the halide ionic radii. Considering this, methylammonium lead perovskites with mixed halide anions, such as $MAPbI_{3-x}Cl_x$ and $MAPbI_{3-x}Br_x$, were synthesized and investigated, resulting in increased stability.[15]

Among a number of synthesized and investigated HOIPs, dimethylammonium lead iodide ($DMAPbI_3$) has garnered significant attention because of its exceptional optoelectronic properties and potential application in high-performance solar cells.[20] García-Fernández *et al.* synthesized two lead halides, as represented by the general formula $DMAPbX_3$ ($X = Cl^-$ and Br^-). Both compounds were found to possess semiconductor characteristics, displaying wide photoluminescent emission and dielectric properties.[21] Mancini *et al.* reported the preparation, single crystal structure determination, and the optical behavior of $APbX_3$ compounds (A = MA, DMA, and TMA; X = I and Br). It was found that crystalized $DMAPbI_3$ belongs to the hexagonal *P6*(3)/*mmc* space group with unit cell parameters of a = 8.769 Å and c = 8.188 Å. Also, their findings revealed improved optical characteristics in these materials.[22] The perovskites doped with $DMAPbCl_{3-x}Br_x$ (with $0 < x < 0.5$), as synthesized by Martínez Muiño *et al.*, exhibit barocaloric features, offering the potential to customize these perovskites to suit a wide range of prospective uses.[23] Pei *et al.*[24] performed a synthesis of $DMAPbX_3$ using DMF as a solvent for PbI_2 and also as a source for dimethylammonium cations due to its hydrolysis in HI. The refined crystal structure of $DMAPbX_3$, obtained by the proposed procedure, was the same as previously reported by Mancini *et al.*[22] In the same paper, the authors reported on mixed $Cs_xDMA_{1-x}PbI_3$ perovskite. By conducting measurements on a single crystal of one-dimensional organic lead iodine perovskite, specifically $DMAPbI_3$, it was determined that $DMAPbI_3$ exhibits ferroelectric properties. This ferroelectric behavior holds the potential to enhance the design of more stable and efficient organometal halide perovskite solar cells and photoelectric devices. Apart from its ferroelectric properties, $DMAPbI_3$ also exhibits blue photoluminescence, making it a promising candidate for multifunctional materials.[25]

Although there is a significant amount of literature data on the synthesis, structure, and properties of the $DMAPbI_3$ perovskite, this compound is still the subject of intense investigations from various perspectives. Therefore, our investigation is focused on the synthesis, characterization, and investigation of the properties of $DMAPbI_3$, specifically its electrochemical behavior and stability. As perovskite-based technologies continue to advance, a comprehensive understanding of their electrochemical behavior becomes paramount. Cyclic voltammetry, a versatile electrochemical technique, offers a valuable means to investigate the redox processes and charge transport mechanisms within these materials.[26] The electrochemical properties of the $DMAPbI_3$ perovskite offer insights into its potential applications in energy storage and conversion devices. The subsequent sections of this article are concerned with the results obtained from the slightly modified synthesis of the $DMAPbI_3$ perovskite, as well as its characterization by PXRD, vibrational spectroscopy, SEM-EDX, and cyclic voltammetry.

2. EXPERIMENTAL SECTION

2.1. *Synthesis*

All initial substances were acquired in analytical grade quality and directly utilized without additional purification from the following suppliers, except for $(CH_3)_2NH_2I$ (DMAI) and PbI_2. Merck provided dimethylamine ($(CH_3)_2NH$, 40 % solution in water), acetonitrile (CH_3CN, > 99 %), and *N*,*N*-dimethylformamide (C_3H_7NO, ≥ 99.8 %), while hydroiodic acid (HI, 57 % *w*/*w* aqueous solution stabilized with 1.5 % H_3PO_2) was sourced from CARLO ERBA Reagents. Ethanol (C_2H_5OH, 96 %) and dichloromethane (CH_2Cl_2, min. 99.0 %) were supplied by Alkaloid. Diethyl ether ($C_4H_{10}O$, ≥ 99.8 %) and tetrabutylammonium chloride ($C_{16}H_{36}ClN$, ≥ 97.0 %) were purchased from Sigma-Aldrich.

The synthesis of dimethylammonium lead iodide ($DMAPbI_3$) comprises a careful procedure of precisely combining dimethylammonium iodide (DMAI) and lead iodide (PbI_2) under controlled conditions. This detailed synthesis description provides a comprehensive overview of the key steps involved in creating $DMAPbI_3$, highlighting the crucial factors influencing the composition, structure, and characteristics of this hybrid organic-inorganic perovskite material.

Dimethylammonium iodide (DMAI, $(CH_3)_2NH_2I$) was synthesized by reacting dimethylamine (DMA, $(CH_3)_2NH_2$) in a slight excess with hydroiodic acid (HI), following a procedure from the literature.[27]

For the synthesis of $(CH_3)_2NH_2PbI_3$ ($DMAPbI_3$) powder, the precursors DMAI

(0.271 g) and PbI_2 (0.723 g) were taken in a 1:1 molar ratio. This mixture was dissolved in a carefully selected solvent, *i.e.*, 15 ml of acetonitrile (ACN), and subjected to thorough stirring to achieve homogeneity. The solvent was carefully removed through controlled evaporation at 60 °C, an important step that initiates the nucleation and growth of $DMAPbI_3$ crystals. After vigorous stirring for 30 minutes, the powder gradually changes color to yellow. Subsequently, the powder is filtered, washed three times with diethyl ether, and the final product is dried at 60 °C in an oven for 12 hours before being stored in a desiccator.

2.2. *Powder X-ray diffraction*

The X-ray diffractograms of the synthesized compounds were recorded on a Rigaku Ultima IV powder X-ray diffractometer (PXRD) with CuKα radiation and a high-speed DetX detector. The diffractograms were recorded at room temperature in the 2θ range from 10° to 80° at a scanning rate of 10°/min.

2.3. *Scanning electron microscopy with energy dispersive X-ray spectroscopy*

Scanning electron microscopy (SEM) of the particles from the studied perovskite was performed with energy dispersive X-ray spectroscopy (EDX). Images and elemental composition were acquired using an FEI Quanta 3D FEG dual beam microscope using an accelerating voltage range of 200 V –30 kV for electron beam imaging and 5–30 kV for ion beam imaging. The samples were placed on a graphite strip and were not adhered (usually gold is used for this) before imaging with the microscope. Recordings were made using an In-lens and/or Everhardt-Thornley secondary electron detector.

2.4. *Infrared spectroscopy*

For the analysis of the infrared spectra of the obtained perovskite, tablets of the sample (about 1 mg) and about 250 mg of KBr were made first. The mixture of KBr and the perovskite sample was stirred and homogenized using a vibrating mixer. Then, the powdered mixture was placed under a press at a pressure of 10 t/cm^2. The infrared spectra of the prepared tablets were recorded on a Perkin Elmer System 2000 FTIR (Fourier-transform infrared spectrometer) in transmission mode. A spectrum of pure KBr was used as a reference spectrum (background spectrum). The samples were recorded at room temperature (25 °C) and –190 °C in the range of 400–4000 cm^{-1}, with each spectrum obtained by averaging 32 scans. To reduce the intensity of the bands originating from atmospheric moisture and CO_2, the software for CO_2/H_2O compensation was used.

2.5. *Raman spectroscopy*

In addition to capturing infrared spectra, Raman spectra of the synthesized perovskites were also obtained. Raman spectra were recorded using a LabRam 300 micro-Raman multichannel spectrometer from Horiba Jobin-Yvon, equipped with a Nd:YAG laser (λ = 632 nm, red laser), and an excitation power of approximately 2.5 mW on the sample. The laser was focused using an OlympusMPla microscope at a magnification of ×50. Recordings were conducted at room temperature, spanning the range of 40–500 cm^{-1}, with an average of 15 scans and a recording time of 5 minutes. A Notch filter was applied to eliminate the Rayleigh incident light and a grating with 1800 lines/mm was utilized to disperse the scattered radiation.

2.6. *Cyclic voltammetry*

The acquisition of cyclic voltammograms was conducted using the μAUTOLAB instrument, specifically model III, manufactured by Autolab in the Netherlands. The electrochemical cell comprised three electrodes: a working electrode, a reference electrode of Ag/Ag^+ (0.1 mol/dm^3) immersed in an acetonitrile solution with TBAC (0.1 mol/dm^3), and an auxiliary electrode made of graphite. The potential of this reference electrode was 0.18 mV more positive than the formal potential of the Fc/Fc^+ redox couple, as obtained from cyclic voltammetry in identical conditions. The working electrode employed was paraffin-impregnated graphite electrode (PIGE) modified with microcrystals of the $DMAPbI_3$ perovskite, which were applied to the electrode surface through abrasion. The solid-state voltammetry of immobilized microparticles was established and thoroughly explained by Sholz *et al.*[28] Here, this technique was performed in non-aqueous solutions. All experiments were performed at room temperature using dichloromethane (DCM) as a solvent and tetrabutylammonium chloride (TBAC) as the supporting electrolyte, with a concentration of 0.1 mol/dm^3. The scan rate (v) for all measurements was 10 mV/s and the step potential (ΔE) was set at 1 mV.

3. RESULTS AND DISCUSSION

3.1. *X-ray diffractogram analysis*

The powder X-ray diffraction (PXRD) pattern of as-synthesized $DMAPbI_3$ perovskite material is presented in Figure 1. The analysis of the diffractogram confirms the purity of the obtained perovskite as the peaks related to lead iodide and dimethylammonium iodide were not observed. The obtained PXRD pattern is consistent with previously reported publications on the crystal structure of crystalline $DMAPbI_3$ [24] that belongs to the space group *P*6(3)*/mmc* with unit cell parameters of a = 8.769 Å and c = 8.188 Å. The lattice parameters calculated from our diffractogram are a = 8.758 Å and c = 8.186 Å.

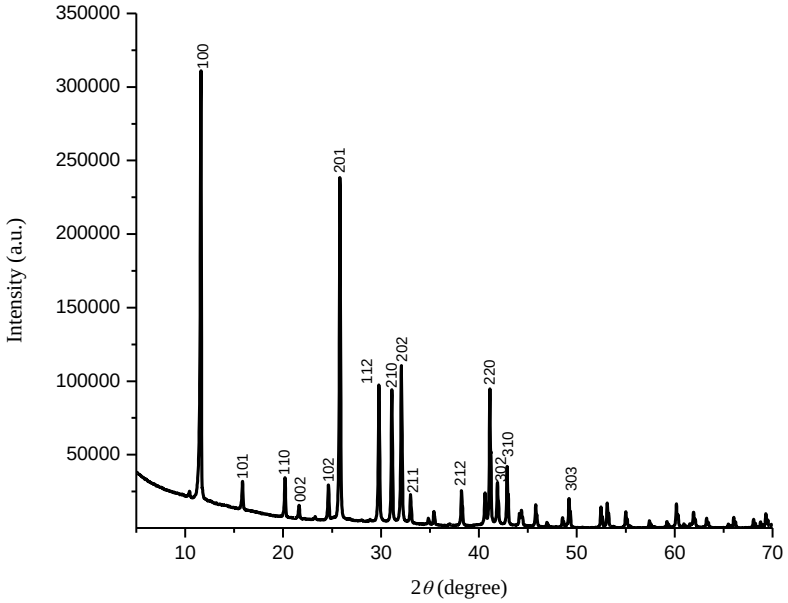

Fig. 1. The X-ray diffraction pattern of the powdered perovskite sample with the given formula $DMAPbI_3$

3.2. *Morphology and elemental composition*

The SEM images of the $DMAPbI_3$ sample (Figs. 2A–C) indicate a porous morphology with rough and dense grains. Most particles are uniform in size and agglomerate to form an open-pore network structure. SEM examinations at different resolutions reveal that the powder particles display a hexagonal rod shape, consistent with the structure of $DMAPbI_3$,[24] and are approximately 1.55 μm wide and 6.95 μm long. The results of the EDX analysis confirm that the sample is homogenous and pure. The composition was confirmed with EDX characteristic peaks corresponding to C, I, and Pb that appear on the EDX spectra. The mass percentages of the heavy elements Pb and I obtained by EDX analysis are in good agreement with the theoretical ones ($w(I)_{EDX}$ = 61.03 %; $w(I)_{theor.}$= 60.05 %; $w(Pb)_{EDX}$ = 30.56 %; and $w(Pb)_{theor.}$ = 32.68 %).

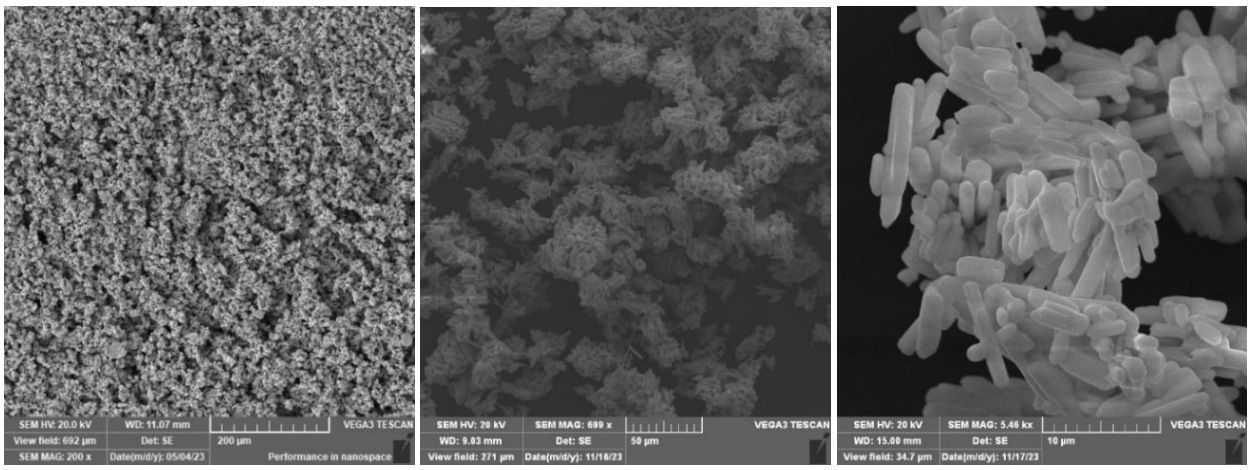

Fig. 2. (**A–C**) SEM images of the $DMAPbI_3$ powder with different resolutions

3.3. *Infrared spectra analysis*

The IR spectra of $DMAPbI_3$ recorded at 25 °C and –190 °C in the range of 600–1650 cm^{-1} are presented in Fig. 3. The bands at 1580 and 1480 cm^{-1} correspond to NH_2 bending modes, with the former originating from NH_2 asymmetric bending and the latter from NH_2 symmetric bending. The bands at 1460 and 1385 cm^{-1} correspond to CH_3 asymmetric and CH_3 symmetric bending modes, respectively. The bands with relatively lower IR intensities at 1232 and 1010 cm^{-1} can be attributed to $(CH_3)_2NH_2^+$ rocking modes and C-N stretching modes, respectively. Proceeding towards lower wavenumber values, two bands at 880 and 840 cm^{-1} are identified, both corresponding to rocking modes of $(CH_3)_2NH_2^+$ (Table 1).

Based on the spectrum recorded at low temperature and the one recorded at room temperature, it is evident that a phase transition occurs in $DMAPbI_3$. The results involving phase transitions in perovskite materials, as published in the literature,[29–31] support the conclusion that there are two different phases present at these two temperatures. The position of the bands and their interchange (especially of the banding CH_3 and the stretching and banding NH_2 vibrations) are clear indications that the phase transition occurs because of the rotation of the CH_3 and NH_2 groups in the crystal structure of the perovskite. They contribute to the changes in the local site symmetry, resulting in the appearance and vanishing of the bands in question.

The broadening of the other bands as the temperature increases is a clear indication of the higher degree of freedom of the organic cations in the structure.

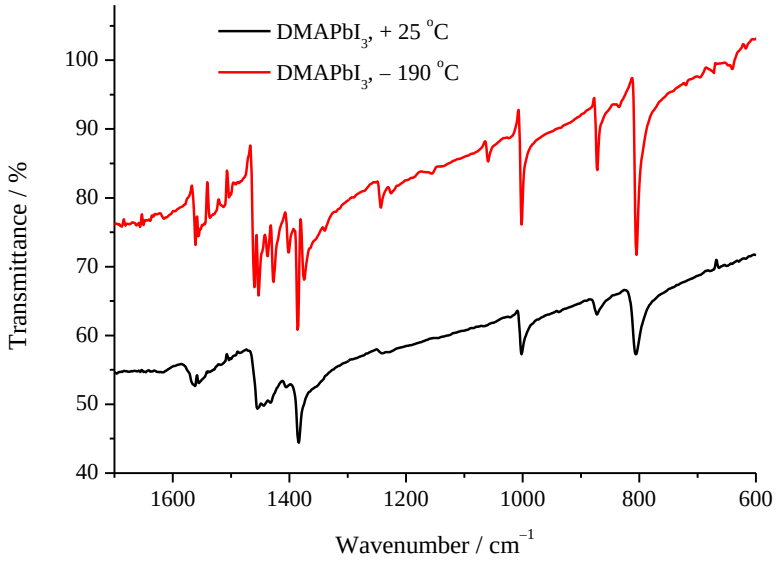

Fig. 3. IR spectra of $DMAPbI_3$ at 25 °C and –190 °C

T a b l e 1

Peak assignments for IR spectroscopy of $DMAPbI_3$ are identified according to ref.[29]

Functional group/ Types of vibration	**Wavenumber (cm^{-1})**	
	Literature	Observed
Asym. NH_2 bending	1650–1580	1580
Sym. NH_2 bending	1550–1480	1480
Asym. CH_3 bending	1470–1450	1460
Sym. CH_3 bending	1385–1370	1385
$(CH_3)_2NH_2^+$ rock	1255–1200	1232
C-N stretch	1250–1000	1010
$(CH_3)_2NH_2^+$ rock	950–850	880
$(CH_3)_2NH_2^+$ rock	950–850	840
Out of plane NH_2 bending	900–650	800

3.4. *Raman spectra analysis*

Figure 4 shows the Raman spectrum of the $DMAPbI_3$ perovskite material at room temperature. The Raman spectra exhibit strong similarities to those documented for hybrid perovskites containing the methylammonium cation $[CH_3NH_3]^+$ (MA) alongside halides such as Br, I, and Cl.[33,34] Usually, the spectra of these compounds are thought to consist of two different parts. First, a low energy band of closely packed Raman peaks, which are commonly intense in the range of 0–200 cm^{-1}, are normally assigned as octahedra vibrational modes (octahedra translation, distortion, and torsion) and organic cation translations (torsion in DMA). Second, and the higher energy modes bands between 200 and 3200 cm^{-1} are usually assigned to organic cation.[34]

Based on the Raman spectrum of this compound, besides the structure determined by XRD, it can be concluded that $DMAPbI_3$ is a one-dimensional perovskite with face-sharing PbI_6 octahedra. This conclusion is based on the absence of the band in the region of 90–96 cm^{-1} (considered to be a combination of multiple modes) as a result of the restrictions in face-sharing structures. On the other hand, the band at 80 cm^{-1} is a result of an in-plane I-Pb-I vibration of the atoms sharing a plane between two octahedra.

A significant challenge in Raman measurements is the presence of a concurrent fluorescence background. The fluorescence intensity is typically much higher than the Raman scattering signal, especially noticeable at higher wavelengths, potentially masking weaker Raman scattering peaks.[35] Fluorescence signals vary in wavelength range, often appearing as broad bands in the visible and short-wave NIR regions, while Raman bands are narrower and more distinguishable.[35–38]

Laser wavelength selection is crucial in Raman excitation. A 785 nm laser for $FAPbI_3$ Raman signal excitation increases the low-frequency Raman background, masking signals below 1000 cm^{-1} due to induced photoluminescence (PL). This interference is particularly pronounced for iodine-rich samples with PL above 785 nm.[40] The same situation is observed in our investigated compound ($DMAPbI_3$) when recorded in the range of 500–4000 cm^{-1} using a red laser line (λ = 632 nm).

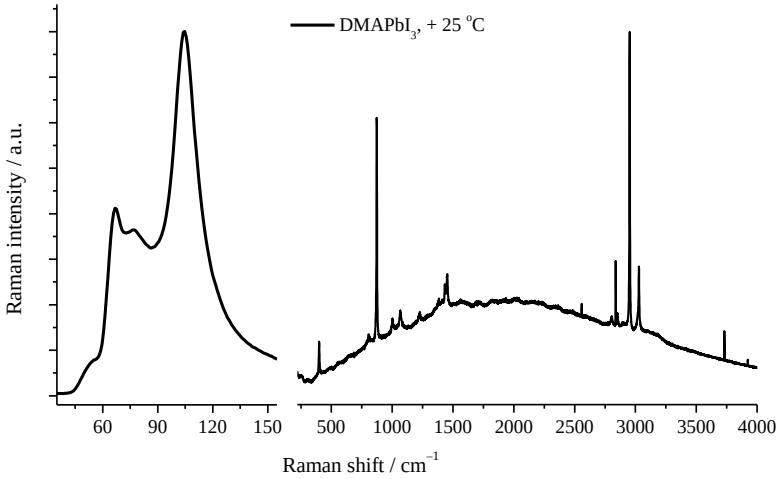

Fig. 4. Raman spectrum of $DMAPbI_3$ at room temperature

3.5. *Cyclic voltammetry*

Although dichloromethane is not a commonly used non-aqueous solvent for electrochemical measurements due to its low permittivity and conductivity, it can offer advantages over other solvents in certain cases. For instance, many solvent/electrolyte pairs were unsuitable for electrochemical measurements of solid particles of $DMAPbI_3$, as the perovskite proved to be unstable. However, it was demonstrated that the perovskite crystals remain stable for extended periods when dichloromethane is utilized, with tetrabutylammonium chloride (TBAC) serving as the supporting electrolyte. Similar findings have been reported in the literature for other related perovskite materials.[41] The cyclic voltammogram of the blank solution (Fig. 5 – grey dotted line) exhibits an oxidation tail beginning at 0.6 V and a reduction tail starting at –1 V.

This current is associated with redox reactions involving both the solvent and electrolyte. Under these conditions, the allowable potential window is approximately 1.6 V, significantly narrower compared to when a Pt electrode was used in dichloromethane.[42] Additionally, the utilization of TBAC also results in a narrowing of the anodic potential

range of the system compared to TBAP (tetrabutylammonium phosphate) or other electrolytes.[43] When the perovskite is immobilized on the PIGE electrode, notable distinctions emerge between the cyclic voltammograms (Fig. 5 – comparing full and dotted lines). Commencing from the open circuit potential (OCP) and going towards positive potentials, the first scan of $DMAPbI_3$ (Fig. 5 – red line) reveals an intense, wide anodic peak initiating at –0.153 V, accompanied by a consistent rise in current throughout the scan. During the reverse scan, a marginal increase in cathodic current begins at –0.11 V and increases further. Evidently, the first scan of $DMAPbI_3$ appears as an electrochemically irreversible process, characterized by a broad peak for oxidation and a minor reduction current.

The second consecutive scan (Fig. 5 – green line) demonstrates a significant reduction in both oxidation and reduction currents, which continues to decrease in the third scan (Fig. 5 – black line). This marked decrease in current during the consecutive scans indicates that after the initial oxidation, the perovskite decomposes into other products and the original perovskite cannot be electrochemically resynthesized. Interestingly, it is shown that the broad oxidation peak in the first scan actually reflects two (or more) electrode reactions that can be seen in the second scan as two separate peaks. All three voltammograms containing the perovskite exhibit lower current tails compared to the blank solution, indicating that the redox reactions involving both the solvent and electrolyte can readily occur on a bare PIGE electrode but are diminished when the perovskite (or other perovskite oxidation products) are present on the electrode.

The voltammograms in Fig. 5 are measured by initial sweeping the potential in a positive potential direction relative to the OCP value. It is evident that $DMAPbI_3$ undergoes oxidation and decomposition. Starting from the OCP at approximately –0.22 V, the cyclic voltammograms of $DMAPbI_3$ were also measured by the initial sweeping of the potential in the negative direction (Fig. 6 – blue line).

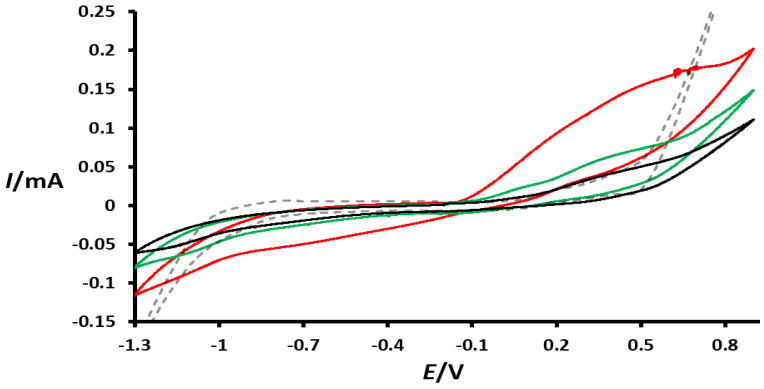

Fig. 5. Cyclic voltammograms of $DMAPbI_3$ particles immobilized on a PIGE electrode showing first (red), second (green), and third (black) consecutive scans compared with a blank solution (grey dotted line). Electrolyte – TBAC (0.1 mol/dm^3) dissolved in dichloromethane; CE – graphite; RE – Ag/Ag^+; v = 10 mV/s; ΔE = 1mV; E_{start} = OCP (open circuit potential)

Within the potential interval from –0.3 to –0.7 V, the reduction current in the blue voltammogram (recorded from the OCP to negative potentials) is lower compared to the voltammogram scanned in the positive direction (Fig. 6 – red line). This indicates that the reduction current at these potentials is primarily caused by the products obtained by oxidation processes taking place at positive potentials, without involving direct reduction of the perovskite. However, at potentials more negative than –0.7 V, the reduction current increases drastically compared to both the voltammogram initially scanned in the positive potential direction and the blank voltammogram (Fig. 6 – grey dotted line). This indicates that the perovskite can be directly reduced. Moreover, after the direct reduction of the perovskite, a new oxidation peak forms around –0.45 V, which was not visible in Figure 5 when the potential was initially scanned in the positive direction. Interestingly, the second and third consecutive scans of the blue voltammogram (data not shown) closely resemble the second and third scans initially scanned in the positive direction (Fig. 5 – green and black lines). Notably, they also lack the peak at –0.45 V, indicating that the perovskite undergoes decomposition into other products after direct reduction, rendering it unable to be electrochemically resynthesized.

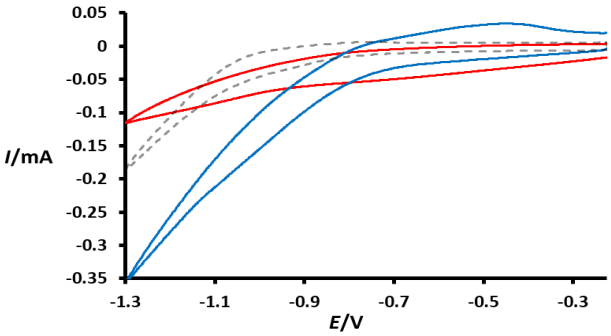

Fig. 6. Cyclic voltammograms of $DMAPbI_3$ particles immobilized on a PIGE electrode scanned from OCP to 1 V in the first scan (red line) and from the OCP to the negative direction (blue line). Additionally, the voltammogram of the blank is displayed for comparison (grey dotted line), as recorded from the OCP to the negative potential direction. All other conditions remain identical to those in Fig. 5.

Assumptions regarding potential oxidation products of the perovskite include the oxidation of the constituents (DMA^+, Pb^{2+}, and I^-) into various forms. The organic cation (DMA^+) may undergo oxidation to different products, eventually leading to CO_2. Lead ions could be oxidized to produce lead oxide, some of which may remain on or fall from the electrode without dissolving. The iodide ion might undergo oxidation to different oxidation states, possibly reaching elemental iodine, although in minute amounts that might not be detectable. After the decomposition of the perovskite, numerous chemical reactions become possible, leading to the production of additional potential candidates for redox reactions. Consequently, it becomes challenging to determine the exact electrode reactions. However, experiments involving other non-perovskite substances containing the constituents of the perovskite (DMA^+, Pb^{2+}, and I^-) under identical conditions (solvent, electrolyte, and electrode) can provide valuable insights (Fig. 7).

The comparison of voltammograms presented in Fig. 7 indicates that the oxidation process starting at –0.15 V for the perovskite (red line) is only observed in samples containing iodine (PbI_2 – blue line in A and DMAI – blue line in B). This observation is further confirmed when I_2 is dissolved in solution (blue line in C). Thus, we can infer that the oxidation processes of the perovskite are primarily associated with the electrochemistry of iodine in dichloromethane. The cyclic voltammogram of $PbCl_2$ (black line in A) exhibits a peak for oxidation at around –0.5 V, which resembles the oxidation peak of $DMAPbI_3$ observed when the perovskite was directly reduced in the initial scan (Fig. 5 – blue line). It is plausible that this peak is linked to the electrochemistry of dissolved oxygen, wherein dissolved oxygen is reduced to form a stable superoxide ion (stable in aprotic solvents), whose oxidation to form oxygen yields an oxidation peak at similar potentials.[44] However, the stability of the superoxide ion and the formation of the peak are intricate and contingent upon factors such as the solvent, the electrolyte, and other ions present in the system (in this case, products of the perovskite electrochemistry).[45]

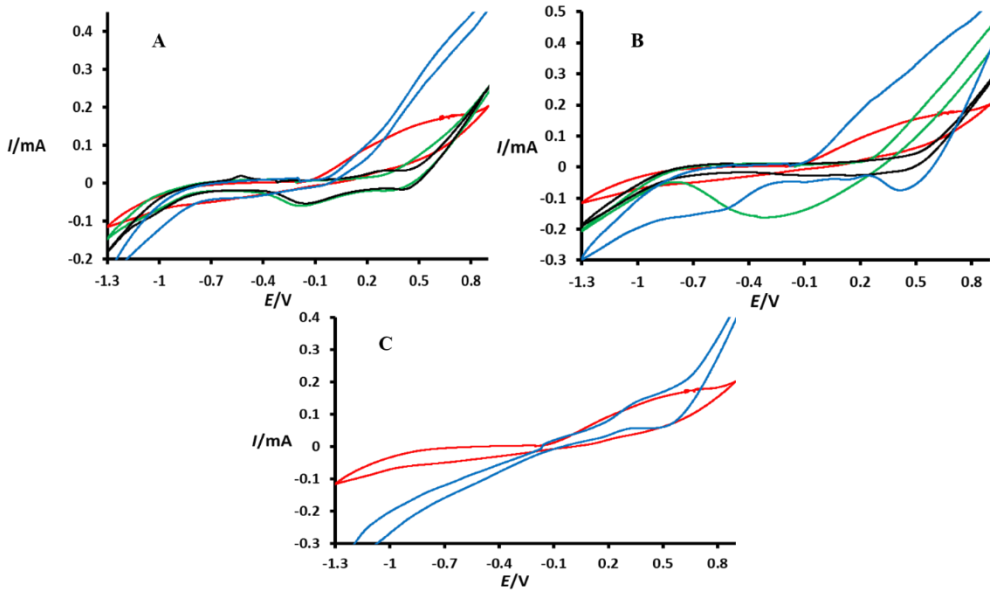

Fig. 7. Cyclic voltammograms of (A) PbX_2 and (B) DMAX particles immobilized on a PIGE, where X = I (blue line), Br (green line), and Cl (black line). Cyclic voltammogram of dissolved I_2 (10^{-3} mol/dm^3, blue line in C). Red curves in all panels show the cyclic voltammograms of $DMAPbI_3$. The potential is scanned initially from the OCP to positive values. All other conditions remain identical to those in Fig. 6.

4. CONCLUSION

Taking into consideration the obtained results in this investigation, several conclusions can be drawn. Hybrid organic-inorganic perovskite $DMAPbI_3$ was successfully obtained via a slightly modified synthesis method compared to the one described in the literature. This was confirmed by a comparison of the recorded PXRD pattern of the obtained product with the previously reported literature data for the structure of $DMAPbI_3$. The IR spectra recorded at –190 °C and at room temperature showed characteristic bands for dimethylammonium cation vibrations. In addition, the comparison of the IR spectra recorded at room temperature and the low temperature indicates a possible phase transition. The Raman spectra align with the spectra reported for similar HOIPs, featuring the low energy band assigned as octahedra vibrational modes associated with torsion in DMA^+, as well as the higher energy modes forming bands between 200 and 3200 cm^{-1} that are usually assigned to organic molecules. The SEM images of $DMAPbI_3$ indicate a porous morphology with rough, dense grains displaying a hexagonal rod shape. The mass percentages for Pb^{2+} and I^- anions obtained by EDX analysis are in good agreement with the theoretical ones. The electrochemical investigation of $DMAPbI_3$, conducted using cyclic voltammetry in dichloromethane (DCM) with tetrabutylammonium chloride (TBAC) as the supporting electrolyte and PIGE as the working electrode, revealed that $DMAPbI_3$ can undergo oxidation and reduction, leading to the decomposition of the perovskite structure and the formation of various potential products. Comparing it with the electrochemistry of other substances containing constituents of $DMAPbI_3$, it was found that the oxidation current is primarily associated with the electrochemistry of iodine in dichloromethane.

REFERENCES

(1) Atta, N. F.; Galal, A.; El-Ads, E. H., *Perovskite Materials – Synthesis, Characterisation, Properties, and Applications*; **2016**. https://doi.org/10.5772/61280.

(2) Tilley, R. J. D., *Perovskites: Structure–Property Relationships*, *MRS Bulletin*, **2017,** *42* (04), 325. https://doi.org/10.1557/MRS.2017.81.

(3) Assirey, E. A. R. Perovskite Synthesis, Properties and Their Related Biochemical and Industrial Application. *Saudi Pharm. J.* **2019**, *27* (6), 817–829. https://doi.org/10.1016/J.JSPS.2019.05.003

(4) Zhang, L.; Mei, L.; Wang, K.; Lv, Y.; Zhang, S.; Lian, Y.; Liu, X.; Ma, Z.; Xiao, G.; Liu, Q.; Zhai, S.; Zhang, S.; Liu, G.; Yuan, L.; Guo, B.; Chen, Z.; Wei, K.; Liu, A.; Yue, S.; Niu, G.; Pan, X.; Sun, J.; Hua, Y.; Wu, W. Q.; Di, D.; Zhao, B.; Tian, J.; Wang, Z.; Yang, Y.; Chu, L.; Yuan, M.; Zeng, H.; Yip, H. L.; Yan, K.; Xu, W.; Zhu, L.; Zhang, W.; Xing, G.; Gao, F.; Ding, L., Advances in the Application of Perovskite Materials. *Nanomicro Lett.* **2023**, *15* (1), 1–48. https://doi.org/10.1007/S40820-023-01140-3

(5) Seok, S. Il; Guo, T. F., Halide Perovskite Materials and Devices. *MRS Bull.* **2020**, *45* (6), 427–430. https://doi.org/10.1557/MRS.2020.140

(6) Cheetham, A. K.; Rao, C. N. R., Materials Science: There's Room in the Middle. *Science (1979)* **2007**, *318* (5847), 58–59. https://doi.org/10.1126/SCIENCE.1147231/ASSET/9F46A027-06B8-41D4-B9A1-66F438B8FF27/ASSETS/SCIENCE.1147231.FP.PNG

(7) Férey, G., Microporous Solids: From Organically Templated Inorganic Skeletons to Hybrid Frameworks ... Ecumenism in Chemistry. *Chem. Mater.* **2001**, *13* (10), 3084–3098. https://doi.org/10.1021/CM011070N

(8) Li, W.; Wang, Z.; Deschler, F.; Gao, S.; Friend, R. H.; Cheetham, A. K., Chemically Diverse and Multifunctional Hybrid Organic–Inorganic Perovskites. *Nat. Rev. Mater.* **2017**, *2* (3), 1–18. https://doi.org/10.1038/natrevmats.2016.99

(9) Weber, D., $CH_3NH_3PbX_3$, Ein Pb(II)-System Mit Kubischer Perowskitstruktur. *Z. Naturforschung B.* **1978**, *33* (12), 1443–1445. https://doi.org/10.1515/ZNB-1978-1214/MACHINEREADABLECITATION/RIS

(10) Mitzi, D. B.; Feild, C. A.; Harrison, W. T. A.; Guloy, A. M., Conducting Tin Halides with a Layered Organic-Based Perovskite Structure. *Nature* **1994**, *369* (6480), 467–469. https://doi.org/10.1038/369467a0

(11) Mitzi, D. B., Templating and Structural Engineering in Organic–Inorganic Perovskites. *J. Chem. Soc., Dalton Transactions* **2001**, No. 1, 1–12. https://doi.org/10.1039/B007070J

(12) Mitzi, D. B.; Wang, S.; Feild, C. A.; Chess, C. A.; Guloy, A. M., Conducting Layered Organic-Inorganic Halides Containing -Oriented Perovskite Sheets. *Science* **1995**, *267* (5203), 1473–1476. https://doi.org/10.1126/SCIENCE.267.5203.1473

(13) Kagan, C. R.; Mitzi, D. B.; Dimitrakopoulos, C. D., Organic-Inorganic Hybrid Materials as Semiconducting Channels in Thin-Film Field-Effect Transistors. *Science (1979)* **1999**, *286* (5441), 945–947. https://doi.org/10.1126/SCIENCE.286.5441.945

(14) Kojima, A.; Teshima, K.; Shirai, Y.; Miyasaka, T., Organometal Halide Perovskites as Visible-Light Sensitizers for Photovoltaic Cells. *J. Am. Chem. Soc.* **2009**, *131* (17), 6050–6051. https://doi.org/10.1021/JA809598R

(15) Wang, Z.; Shi, Z.; Li, T.; Chen, Y.; Huang, W., Stability of Perovskite Solar Cells: A Prospective on the Substitution of the A Cation and X Anion. *Angew. Chem. Int. Ed. Engl.* **2017**, *56* (5), 1190–1212. https://doi.org/10.1002/ANIE.201603694

(16) Pellet, N.; Gao, P.; Gregori, G.; Yang, T. Y.; Nazeeruddin, M. K.; Maier, J.; Grätzel, M., Mixed-Organic-

Cation Perovskite Photovoltaics for Enhanced Solar-Light Harvesting. *Angew. Chem. Int. Ed. Engl.* **2014**, *53* (12), 3151–3157. https://doi.org/10.1002/ANIE.201309361

(17) Zou, S.; Liu, Y.; Li, J.; Liu, C.; Feng, R.; Jiang, F.; Li, Y.; Song, J.; Zeng, H.; Hong, M.; Chen, X., Stabilizing Cesium Lead Halide Perovskite Lattice through Mn(II) Substitution for Air-Stable Light-Emitting Diodes. *J. Am. Chem. Soc.* **2017**, *139* (33), 11443–11450. https://doi.org/10.1021/JACS.7B04000/SUPPL_FILE/JA7B04000_SI_001.PDF

(18) Futscher, M. H.; Gangishetty, M. K.; Congreve, D. N.; Ehrler, B., Quantifying Mobile Ions and Electronic Defects in Perovskite-Based Devices with Temperature-Dependent Capacitance Measurements: Frequency vs Time Domain. *J. Chem. Phys.* **2020**, *152* (4). https://doi.org/10.1063/1.5132754.

(19) Liu, Y.; Yang, Z.; Cui, D.; Ren, X.; Sun, J.; Liu, X.; Zhang, J.; Wei, Q.; Fan, H.; Yu, F.; Zhang, X.; Zhao, C.; Liu, S., Two-Inch-Sized Perovskite $CH_3NH_3PbX_3$ (X = Cl, Br, I) Crystals: Growth and Characterization. *Adv. Mater.* **2015**, *27* (35), 5176–5183. https://doi.org/10.1002/ADMA.201502597

(20) Quarti, C.; Mosconi, E.; Ball, J. M.; D'Innocenzo, V.; Tao, C.; Pathak, S.; Snaith, H. J.; Petrozza, A.; De Angelis, F., Structural and Optical Properties of Methylammonium Lead Iodide across the Tetragonal to Cubic Phase Transition: Implications for Perovskite Solar Cells. *Energy Environ. Sci.***2016**, *9* (1), 155–163. https://doi.org/10.1039/C5EE02925B

(21) García-Fernández, A.; Juarez-Perez, E. J.; Bermúdez-García, J. M.; Llamas-Saiz, A. L.; Artiaga, R.; López-Beceiro, J. J.; Señarís-Rodríguez, M. A.; Sánchez-Andújar, M.; Castro-García, S., Hybrid Lead Halide $[(CH_3)_2NH_2]PbX_3$ (X = Cl^- and Br^-) Hexagonal Perovskites with Multiple Functional Properties. *J. Mater. Chem. C. Mater.* **2019**, *7* (32), 10008–10018. https://doi.org/10.1039/C9TC03543E

(22) Mancini, A.; Quadrelli, P.; Amoroso, G.; Milanese, C.; Boiocchi, M.; Sironi, A.; Patrini, M.; Guizzetti, G.; Malavasi, L., Synthesis, Structural and Optical Characterization of $APbX_3$ (A=methylammonium, Dimethylammonium, Trimethylammonium; X = I, Br, Cl) Hybrid Organic-Inorganic Materials. *J. Solid State Chem.* **2016**, *240*, 55–60. https://doi.org/10.1016/J.JSSC.2016.05.015

(23) Martínez Muiño, A., Synthesis and Study of New Materials with Barocaloric Properties. *I Premio UDC Sustentabilidade a traballos fin de grao e mestrado 2018, ISBN 978-84-9749-783-1,* **2019**, 89–102.

(24) Pei, Y.; Liu, Y.; Li, F.; Bai, S.; Jian, X.; Liu, M., Unveiling Property of Hydrolysis-Derived $DMAPbI_3$ for Perovskite Devices: Composition Engineering, Defect Mitigation, and Stability Optimization. *iScience* **2019**, *15*, 165–172. https://doi.org/10.1016/J.ISCI.2019.04.024

(25) Wang, Y.; Liu, Y.; Wu, Y.; Jiang, J.; Liu, C.; Liu, W.; Gao, K.; Cai, H.; Wu, X. S., Properties and Growth of Large Single Crystals of One-Dimensional Organic Lead Iodine Perovskite. *Cryst. Eng. Comm.* **2020**, *22* (42), 7090–7094. https://doi.org/10.1039/D0CE01104E

(26) Elgrishi, N.; Rountree, K. J.; McCarthy, B. D.; Rountree, E. S.; Eisenhart, T. T.; Dempsey, J. L., A Practical Beginner's Guide to Cyclic Voltammetry. *J. Chem. Educ.* **2018**, *95* (2), 197–206. https://doi.org/10.1021/ACS.JCHEMED.7B00361/SUPPL_FILE/ED7B00361_SI_002.DOCX

(27) Bukleski, M.; Dimitrovska-Lazova, S.; Aleksovska, S., Vibrational Spectra of Methylammonium Iodide and Formamidinium Iodide in a Wide Temperature Range. *Maced. J. Chem. Chem. Eng.* **2019**, *38* (2), 237–252. https://doi.org/10.20450/MJCCE.2019.1940

(28) Scholz, F.; Schröder, U.; Gulaboski, R., *Electrochemistry of Immobilized Particles and Droplets*; **2005**, 1–290. https://doi.org/10.1007/B137048.

(29) Pérez-Osorio, M. A.; Milot, R. L.; Filip, M. R.; Patel, J. B.; Herz, L. M.; Johnston, M. B.; Giustino, F., Vibrational Properties of the Organic-Inorganic Halide Perovskite $CH_3NH_3PbI_3$ from Theory and Experiment: Factor Group Analysis, First-Principles Calculations, and Low-Temperature Infrared Spectra. *J. Phys. Chem. C.* **2015**, *119* (46), 25703–25718. https://doi.org/10.1021/ACS.JPCC.5B07432

(30) Dimitrovska-Lazova, S.; Bukleski, M.; Tzvetkov, P.; Pecovska-Gjorgjevich, M.; Kovacheva, D.; Aleksovska, S., The Mechanism of the Isostructural Phase Transition in $C(NH_2)_3PbI_3$ as a Guide for Understanding the Properties of the New Phase. *Mater. Chem. Phys.* **2022**, *275*, 125240. https://doi.org/10.1016/J.MATCHEMPHYS.2021.125240

(31) Bukleski, M.; Dimitrovska-Lazova, S.; Aleksovska, S., Temperature Dependent Phase Transitions and Their Relation to Isosbestic Point Formation. Case Study of $C(NH_2)_3PbI_3$. *Spectrochim. Acta. A. Mol. Biomol. Spectrosc.* **2022**, *266*, 120462. https://doi.org/10.1016/J.SAA.2021.120462

(32) Bukleski, M.; Dimitrovska-Lazova, S.; Makrievski, V.; Aleksovska, S., A Simple Approach for Determination of the Phase Transition Temperature Using Infrared Temperature-Induced Isosbestic Points. *Spectrochim. Acta. A. Mol. Biomol. Spectrosc.* **2020**, *231*, 118118. https://doi.org/10.1016/J.SAA.2020.118118

(33) Leguy, A. M. A.; Goñi, A. R.; Frost, J. M.; Skelton, J.; Brivio, F.; Rodríguez-Martínez, X.; Weber, O. J.; Pallipurath, A.; Alonso, M. I.; Campoy-Quiles, M.; Weller, M. T.; Nelson, J.; Walsh, A.; Barnes, P. R. F., Dynamic Disorder, Phonon Lifetimes, and the Assignment of Modes to the Vibrational Spectra of Methylammonium Lead Halide Perovskites. *Phys. Chem. Chem. Phys.* **2016**, *18* (39), 27051–27066. https://doi.org/10.1039/C6CP03474H

(34) Gjorgjevikj, K.; Bukleski, M.; Dimitrovska-Lazova, S.; Aleksovska, S., Raman Spectroscopy as a Tool for Predicting the Dimensionality and Octahedra Connectivity in Lead Iodide Perovskites. *J. Mol. Struct.* **2023**, *1293*, 136236. https://doi.org/10.1016/J.MOLSTRUC.2023.136236

(35) Wei, D., Chen S., Liu Q., Review of Fluorescence Suppression Techniques in Raman Spectroscopy. **2024**. https://doi.org/10.1080/05704928.2014.999936

(36) Vickers, T. J.; Wambles, R. E.; Mann, C. K., Curve Fitting and Linearity: Data Processing in Raman Spectroscopy. *Appl. Spectrosc.* **2001**, *55* (4), 389–393. https://doi.org/10.1366/0003702011952127

(37) O'Grady, A.; Dennis, A. C.; Denvir, D.; McGarvey, J. J.; Bell, S. E. J., Quantitative Raman Spectroscopy of Highly Fluorescent Samples Using Pseudosecond De-

rivatives and Multivariate Analysis. *Anal. Chem.* **2001**, *73(9)* (9), 2058–2065. https://doi.org/10.1021/AC0010072

(38) Zhao, J.; Carrabba, M. M.; Allen, F. S., Automated Fluorescence Rejection Using Shifted Excitation Raman Difference Spectroscopy. **2002**, *56* (7), 834–845. https://doi.org/10.1366/000370202760171491

(39) Mahadevan-Jansen, A.; Lieber, C. A., Automated Method for Subtraction of Fluorescence from Biological Raman Spectra. *Appl. Spectrosc.* **2003**, *57* (11), 1363–1367. https://doi.org/10.1366/000370203322554518

(40) Ruan, S.; McMeekin, D. P.; Fan, R.; Webster, N. A. S.; Ebendorff-Heidepriem, H.; Cheng, Y. B.; Lu, J.; Ruan, Y.; McNeill, C. R., Raman Spectroscopy of Formamidinium-Based Lead Halide Perovskite Single Crystals. *J. Phys. Chem. C.* **2020**, *124* (4), 2265–2272. https://doi.org/10.1021/ACS.JPCC.9B08917/SUPPL_FILE/JP9B08917_SI_001.PDF

(41) Samu, G. F.; Scheidt, R. A.; Kamat, P. V.; Janáky, C., Electrochemistry and Spectroelectrochemistry of Lead Halide Perovskite Films: Materials Science Aspects and Boundary Conditions. *Chem. Mater.* **2018**, *30* (3), 561–569. https://doi.org/10.1021/ACS.CHEMMATER.7B04321/ASSET/IMAGES/LARGE/CM-2017-04321D_0007.JPEG

(42) *Electroanalytical Chemistry. A Series of Advances.* Volume 8 by Bard, Allen J., ed.: Good (1975) | Zubal-Books, Since 1961. https://www.abebooks.com/servlet/BookDetailsPL?bi=13362053353&cm_sp=rec-_-pd_hw_i_1-_-bdp&ref_=pd_hw_i_1 (accessed 2024-03-12)

(43) Kadish, K. M.; Anderson, J. E., Purification of Solvents for Electroanalysis: Benzonitile. *Pure Appl. Chem.* **1987**, *59* (5), 703–714. https://doi.org/10.1351/PAC198759050703/PDF

(44) Huango, X. J.; Rogers, E. I.; Hardacre, C.; Compton, R. G., The Reduction of Oxygen in Various Room Temperature Ionic Liquids in the Temperature Range 293-318 K: Exploring the Applicability of the Stokes-Einstein Relationship in Room Temperature Ionic Liquids. *J. Phys. Chem. B.* **2009**, *113* (26), 8953–8959. https://doi.org/10.1021/JP903148W/SUPPL_FILE/JP903148W_SI_001.PDF

(45) Hayyan, M.; Hashim, M. A.; Alnashef, I. M., Superoxide Ion: Generation and Chemical Implications. *Chem. Rev.* **2016**, *116* (5), 3029–3085. https://doi.org/10.1021/ACS.CHEMREV.5B00407